Numerical simulation of wave-induced fluid flow seismic attenuation based on the Cole-Cole model

Stefano Picotti[a] and José M. Carcione
Istituto Nazionale di Oceanografia e di Geofisica Sperimentale (OGS), Borgo Grotta Gigante 42c, 34010 Sgonico, Trieste, Italy

(Received 7 April 2017; revised 3 June 2017; accepted 17 June 2017; published online 12 July 2017)

The acoustic behavior of porous media can be simulated more realistically using a stress-strain relation based on the Cole-Cole model. In particular, seismic velocity dispersion and attenuation in porous rocks is well described by mesoscopic-loss models. Using the Zener model to simulate wave propagation is a rough approximation, while the Cole-Cole model provides an optimal description of the physics. Here, a time-domain algorithm is proposed based on the Grünwald-Letnikov numerical approximation of the fractional derivative involved in the time-domain representation of the Cole-Cole model, while the spatial derivatives are computed with the Fourier pseudospectral method. The numerical solution is successfully tested against an analytical solution. The methodology is applied to a model of saline aquifer, where carbon dioxide (CO_2) is injected. To follow the migration of the gas and detect possible leakages, seismic monitoring surveys should be carried out periodically. To this aim, the sensitivity of the seismic method must be carefully assessed for the specific case. The simulated test considers a possible leakage in the overburden, above the caprock, where the sandstone is partially saturated with gas and brine. The numerical examples illustrate the implementation of the theory. © *2017 Acoustical Society of America*.
[http://dx.doi.org/10.1121/1.4990965]

[RKS] Pages: 134–145

I. INTRODUCTION

Local fluid flow explains the high attenuation of low-frequency waves in fluid-saturated rocks. When seismic waves propagate through small-scale heterogeneities, pressure gradients are induced between regions of dissimilar properties. White *et al.* (1975) and Johnson (2001) have shown that attenuation and velocity dispersion measurements can be explained by the combined effect of mesoscopic-scale inhomogeneities and energy transfer between wave modes, with P-wave to slow P (Biot)-wave conversion being the main physical mechanism. We refer to this mechanism as mesoscopic loss. The mesoscopic-scale length is intended to be larger than the grain sizes but much smaller than the wavelength of the pulse. For instance, if the matrix porosity varies significantly from point to point, diffusion of pore fluid between different regions constitutes a mechanism that can be important at seismic frequencies. A review of the different theories and authors, who have contributed to the understanding of this mechanism, can be found, for instance, in Carcione and Picotti (2006) and Carcione (2014).

The Cole-Cole model has been used to describe attenuation by Spencer (1981) who conducted forced-deformation experiments at frequencies from 4 to 400 Hz in fluid-saturated sandstones and limestones, implying a stress-relaxation mechanism in the presence of pore fluids. More recently, Lu and Hanyga (2004) simulated wave propagation in viscoelastic media using the Cole-Cole model and fractional time derivatives. These works provide a phenomenological description of wave loss. The Cole-Cole model has also been used to model the deformation of rocks by pressure solution, to simulate the seismoelectric coupling in a poroelastic body saturated by a viscoelastic fluid and to model the complex conductivity of porous media (Revil and Jardani, 2010; Revil *et al.*, 2006; Revil *et al.*, 2014). Here, we show that the Cole-Cole model can be linked to a physical process such as wave-induced fluid flow.

Simulation of synthetic seismograms in the presence of mesoscopic loss requires solving Biot's differential equations (e.g., Picotti *et al.*, 2007). Because the loss mechanism involves the conversion of fast P-wave energy to diffusion energy in the form of the Biot slow wave and the wavelength of this wave can be very small, the poroelastic solution requires a very large amount of storage and computer time. An efficient approach is to approximate the attenuation and velocity dispersion curves using a viscoelastic model and then solve the corresponding differential equations. Picotti *et al.* (2010) and Picotti *et al.* (2012) attempted to approximate the mesoscopic loss in partially saturated rocks by using the Zener viscoelastic model. This model provides accurate fits when the gas patches have a regular geometry. On the other hand, the fit is not good for irregular geometries. An optimal agreement is obtained with the Cole-Cole model, which has been introduced in electromagnetism [Cole and Cole, 1941; Carcione, 2014, Eq. (8.138)]. In this field of research, Abdullah *et al.* (2012), Rekanos and Yioultsis (2014), and Bia *et al.* (2015) have solved the electromagnetic equations using different techniques to compute the fractional derivative.

As the Zener kernel is a good approximation to both the Biot loss mechanism (Carcione, 1998, 2014) and the squirt-flow dissipation peak and related velocity dispersion

[a]Electronic mail: spicotti@inogs.it

(Carcione and Gurevich, 2011), the Cole-Cole kernel provides a good fit to the White and Johnson mesoscopic models. In particular, the Johnson model has two relevant parameters determining the shape and the mean size of the patches, which makes it more general than the White model based on spherical shapes. For a single relaxation mechanism, such as pore fluids oscillating in a general porous medium, the compressional wave will show a sigmoidal increase with increasing frequency and attenuation will peak at the relaxation frequency, where velocity increases rapidly. This coupling can be described by a Cole-Cole model (e.g., Batzle *et al.*, 2006).

Here, we propose to solve the time-domain differential equations based on the Cole-Cole model with a direct method, where the spatial derivatives are computed by using the staggered Fourier pseudospectral method (e.g., Carcione, 2014). Fractional time derivatives are computed with the Grünwald-Letnikov (GL) approximation (Carcione *et al.*, 2002; Caputo *et al.*, 2011), which is an extension of the standard finite-difference approximation for derivatives of integer order.

In the first part of this work, we introduce the stress-strain relation and Johnson model, and calculate the complex moduli, phase velocities, and quality factors versus frequency. We then recast the wave equation in the time-domain in terms of fractional derivatives and obtain the GL approximation. The model is discretized on a mesh, and the spatial derivatives are calculated with the Fourier method by using the fast Fourier transform.

The methodology is applied to the problem of CO_2 storage monitoring. Specifically, we consider a model of saline aquifer, where CO_2 is injected. Besides following the migration of the plume in the reservoir, the objective of monitoring is the detection of possible CO_2 leakages in the above formations. Picotti *et al.* (2012) assessed the sensitivity of the reflection seismic method from the surface for this specific problem, by using Zener approximations. Use of the Cole-Cole model could allow for more reliable sensitivity studies. To estimate the amount of leaked gas, it is essential to fully characterize the seismic properties of the formations constituting the caprock and overburden. We consider a possible leakage scenario in the overburden, caused by the degradation of the casing of an abandoned well.

II. MESOSCOPIC-LOSS MODELS OF PATCHY SATURATION

White (1975) and White *et al.* (1975) were the first to introduce the mesoscopic-loss mechanism based on approximations in the framework of Biot theory. Their first model consisted of porous layers alternately saturated with water and gas, respectively, where the layers might be also composed of different materials. Then, they considered a periodic ensemble of spherical gas pockets in a water-saturated porous medium. In recent studies (Johnson, 2001; Müller and Gurevich, 2005) a generalization of White model for patches of arbitrary shape was developed. In particular, Johnson (2001) obtained the P-wave modulus $E(\omega)$, where ω is the angular frequency, to describe the crossover between the high and low frequency limits. The theory of $E(\omega)$ is extensively outlined in Appendix A [Eq. (A14)], while a review of White's layered model is given in Appendix B. In addition to the usual parameters of Biot theory, Johnson model of patchy saturation has two other parameters, depending on the patch geometry. These parameters are the specific surface area S/V (the ratio of the surface area of a patch to its volume, referred to as *shape factor*), which depends on the shape of the patches, and the parameter T (referred to as *size factor*), which is governed by the mean size of the patches. For a given shape, Johnson (2001) derived asymptotic solutions for low and high frequencies. The two parameters S/V and T appear in the expressions for the high and low frequency limits. The solution for intermediate frequencies was proposed using the simplest function that ensured causality of the solution (Johnson, 2001). A review of the theory of White and Johnson models can also be found in Picotti *et al.* (2010).

III. THE COLE-COLE MODEL

Effective attenuation can be described by means of power laws in the form of fractional derivatives. With the purpose of obtaining the equivalent viscoelastic medium, we use the Cole-Cole model (Cole and Cole, 1941; Bagley and Torvik, 1986; Hanyga, 2003; Bano, 2004; Carcione, 2014), which has been adopted to describe dispersion and energy loss in dielectrics, anelastic media and electric networks (e.g., Grimnesand and Martinsen, 2005). The frequency-domain Cole-Cole stress-strain relation (based on irrational powers of the frequency) can be represented in the time domain as a differential equation involving derivatives of fractional order (e.g., Carcione, 2014). The complex modulus of a Cole-Cole element can be expressed as

$$M(\omega) = M_U \left(\frac{\tau_\sigma}{\tau_\epsilon}\right)^q \left[\frac{1+(\mathrm{i}\omega\tau_\epsilon)^q}{1+(\mathrm{i}\omega\tau_\sigma)^q}\right], \tag{1}$$

where M_U is the unrelaxed (high-frequency) modulus, τ_σ and τ_ε are relaxation times, $0 \le q < 2$ is a real number and $\mathrm{i} = \sqrt{-1}$ is the imaginary number. When $q = 1$, we obtain the Zener model (e.g., Picotti *et al.*, 2010; Carcione, 2014), while $q = 0$ gives the lossless case. The quality factor associated with M is equal to $\mathrm{Re}(M)/\mathrm{Im}(M)$, where Re and Im denote real and imaginary parts. Its minimum value is located at

$$\omega_0 = \frac{1}{\sqrt{\tau_\sigma \tau_\epsilon}} \tag{2}$$

and is equal to

$$Q_0 = \frac{(1+\gamma^2)\cot\varphi + 2\gamma\csc\varphi}{\gamma^2 - 1}, \quad \gamma = \left(\frac{\tau_\epsilon}{\tau_\sigma}\right)^{q/2}, \quad \varphi = \frac{\pi q}{2}. \tag{3}$$

$f_0 = \omega_0/(2\pi)$ is the central frequency of the relaxation peak, and $1/Q_0$ is the maximum dissipation factor (e.g., Carcione, 2014).

Using ω_0 and Q_0 as parameters, we have

$$\tau_\epsilon = \frac{\gamma^{1/q}}{\omega_0}, \quad \tau_\sigma = \frac{\gamma^{-1/q}}{\omega_0}, \tag{4}$$

where γ is a solution of Eq. (3),

$$\gamma = \frac{1 + \sqrt{1 + Q_0^2}\sin\varphi}{Q_0 \sin\varphi - \cos\varphi}. \tag{5}$$

The Cole-Cole model stress (σ)-strain (ε) relation, corresponding to the kernel (1), is

$$\sigma + \tau_\sigma^q \frac{\partial^q \sigma}{\partial t^q} = M_R\left(\epsilon + \tau_\epsilon^q \frac{\partial^q \epsilon}{\partial t^q}\right), \quad 0 \le q < 2, \tag{6}$$

where

$$M_R = M_U\left(\frac{\tau_\sigma}{\tau_\epsilon}\right)^q \tag{7}$$

is the relaxed (low-frequency) modulus (e.g., Carcione, 2014). The limit $q = 1$ gives the Zener model and $\tau_\varepsilon = 0$ gives the Kelvin-Voigt model implemented in Caputo *et al.* (2011). In the frequency domain, we have

$$\sigma = M\epsilon. \tag{8}$$

IV. PHASE VELOCITY AND QUALITY FACTOR

The complex velocity is the key quantity to obtain the phase velocity and quality factor of the equivalent viscoelastic medium. The complex P-wave velocities are

$$v(\omega) = \sqrt{\frac{E(\omega)}{\rho}} \quad \text{and} \quad \bar{v}(\omega) = \sqrt{\frac{M(\omega)}{\rho}} \tag{9}$$

for the Johnson and Cole-Cole models, respectively. The bulk density is

$$\rho = (1 - \phi)\rho_s + \phi\rho_f, \tag{10}$$

where ρ_s is the grain density and ϕ is the porosity. The density of the fluid mixture is

$$\rho_f = S_1\rho_{f1} + S_2\rho_{f2}, \quad S_2 = 1 - S_1, \tag{11}$$

where ρ_{fj} is the density of the jth fluid (i.e., gas and water), and S_j, $j = 1$, 2, the corresponding saturation. The phase velocity and quality factor are

$$v_p = \left[\mathrm{Re}\left(\frac{1}{v}\right)\right]^{-1} \tag{12}$$

and

$$Q = \frac{\mathrm{Re}(v^2)}{\mathrm{Im}(v^2)} \tag{13}$$

(e.g., Carcione, 2014). The properties of the Cole-Cole model are obtained by replacing v by $\bar{v}$.

V. 2D DYNAMICAL EQUATIONS

The conservation of linear momentum for a 2D linear anelastic medium, describing dilatational deformations, can be written as

$$\rho\partial_t^2 u_i = \partial_i \sigma, \quad i = 1(x), 2(y), \tag{14}$$

where u_i are displacement components and ∂_t and ∂_i denote partial time and spatial derivatives, respectively.

The initial conditions are $u_i(0, \mathbf{x}) = 0$, $\partial_t u_i(0, \mathbf{x}) = 0$, and $u_i(t, \mathbf{x}) = 0$, for $t < 0$, where $\mathbf{x}$ is the position vector. The strain-displacement relation is $\epsilon = \partial_1 u_1 + \partial_2 u_2$. Then, the complete set of equations describing the propagation is

$$\begin{aligned}
&\partial_t^2 u_1 = \rho^{-1}\partial_1 \sigma,\\
&\partial_t^2 u_2 = \rho^{-1}\partial_2 \sigma,\\
&\sigma + \tau_\sigma^q \frac{\partial^q \sigma}{\partial t^q} = M_R\left(\epsilon + \tau_\epsilon^q \frac{\partial^q \epsilon}{\partial t^q}\right),\\
&\epsilon = \partial_1 u_1 + \partial_2 u_2.
\end{aligned} \tag{15}$$

VI. NUMERICAL ALGORITHM

The computation of the fractional derivative is based on the Grünwald-Letnikov (GL) approximation (Podlubny, 1999; Carcione *et al.*, 2002). The fractional derivative of order q of a function g is

$$\frac{\partial^q g}{\partial t^q} \approx D^q g = \frac{1}{h^q}\sum_{j=0}^{J} (-1)^j \binom{q}{j} g(t - jh), \tag{16}$$

where h is the time step, and $J = t/h - 1$. The derivation of this expression can be found, for instance, in Carcione *et al.* (2002). The fractional derivative of g at time t depends on all the previous values of g. This is the memory property of the fractional derivative, related to field attenuation. The binomial coefficients are negligible for j exceeding an integer J. This allows us to truncate the sum at $j = L$, $L \le J$, where L is the effective memory length.

Fractional derivatives of order $q < 1$ require large memory resources and computational time, because the decay of the binomial coefficients in Eq. (16) is slow (Carcione *et al.*, 2002; Carcione, 2009), and the effective memory length L is large. We increase the order of the derivative by applying a time derivative of order m to the third Eq. (15). The result is

$$\begin{aligned}
&\partial_t^2 u_1 = \rho^{-1}\partial_1 \sigma,\\
&\partial_t^2 u_2 = \rho^{-1}\partial_2 \sigma,\\
&D^m\sigma + \tau_\sigma^q D^{m+q}\sigma = M_R(D^m\epsilon + \tau_\epsilon^q D^{m+q}\epsilon) + s,\\
&\epsilon = \partial_1 u_1 + \partial_2 u_2,
\end{aligned} \tag{17}$$

where we added a source term s. It is enough to take $m = 1$ to have a considerable saving in memory storage compared to $m = 0$.

We discretize Eq. (17) at $t = nh$. Using the notation $u^n = u(nh)$, the left-hand side of the first two expressions in Eq. (17) can be approximated using

$$h^2 (D^2 u_i)^n = u_i^{n+1} - 2u_i^n + u_i^{n-1}, \quad i = 1, 2, \tag{18}$$

where we have used a right-shifted finite-difference expression for the second derivative. The third equation results in

$$\sigma^n = M_R(\epsilon^n + \Sigma_\epsilon + h^m \tau_\epsilon^q D_\epsilon^{q+m}) - \Sigma_\sigma - h^m \tau_\sigma^q D_\sigma^{q+m}, \tag{19}$$

where

$$\Sigma_\xi = \sum_{j=1}^{m} (-1)^j \binom{m}{j} \xi^{m-j}. \tag{20}$$

Let us consider the case $m = 1$. The GL derivative (16) at time nh can be rewritten as

$$\begin{aligned} D^{q+1} g^n &= \frac{g^n}{h^{q+1}} + r_g^{(q+1)}, \\ r_g^{(q+1)} &= \frac{1}{h^{q+1}} \sum_{j=1}^{J} (-1)^j \binom{q+1}{j} g^{n-j}, \end{aligned} \tag{21}$$

where $r_g^{(q+1)}$ has the memory of the field from $n-1$ and back in time.

Finally, we obtain

$$\begin{aligned} u_1^{n+1} &= h^2 \left(\rho^{-1} \partial_1 \sigma^n\right) + 2u_1^n - u_1^{n-1}, \\ u_2^{n+1} &= h^2 \left(\rho^{-1} \partial_2 \sigma^n\right) + 2u_2^n - 3u_2^{n-1}, \\ \sigma^n &= \frac{1}{a_\sigma} \left[\sigma^{n-1} - h\tau_\sigma^q r_\sigma^{q+1} + M_R \left(a_\epsilon \epsilon^n - \epsilon^{n-1} \right.\right. \\ &\quad \left.\left. + h\tau_\epsilon^q r_\epsilon^{q+1}\right) + hs^n\right], \\ \epsilon^n &= \partial_1 u_1^n + \partial_2 u_2^n, \end{aligned} \tag{22}$$

where

$$a_\xi = 1 + \left(\frac{\tau_\xi}{h}\right)^q, \quad \xi = \epsilon, \sigma. \tag{23}$$

The spatial derivatives are calculated with the staggered Fourier method by using the fast Fourier transform (FFT) (Carcione, 1999, 2009, 2014). The Fourier pseudospectral method has spectral accuracy for band-limited signals. Then, the results are not affected by spatial numerical dispersion. Grid staggering requires averaging the material properties to remove diffractions arising from the discretization of the interfaces. At half-grid points, we average the values defined at regular points. In this case, we apply an arithmetic averaging to the density and the stiffness.

Since we use Fourier basis functions to compute the spatial derivatives, Eq. (22) satisfies periodic boundary conditions at the edges of the numerical mesh.

VII. MATRIX AND FLUID PROPERTIES

Permeability can be related to porosity by the Kozeny-Carman relation

$$\kappa = \frac{B\phi^3 D^2}{(1-\phi)^2} \tag{24}$$

(Mavko *et al.*, 1998), where D is the grain diameter and $B = 0.003$. Equation (24) is an approximation of the permeability of porous media, which is sufficient for the objectives of the present work. However, other theories can better capture the effects of the heterogeneities in the permeability computation (e.g., Revil and Florsch, 2010). We use the Krief model (Krief *et al.*, 1990) to obtain the dry-rock moduli K_m and μ_m. The porosity dependence is consistent with the concept of critical porosity, since the moduli should be small above a certain value of the porosity (usually from 0.4 to 0.6). The moduli are given by

$$\begin{aligned} K_m &= K_s (1-\phi)^{3/(1-\phi)}, \\ \mu_m &= K_m \mu_s / K_s, \end{aligned} \tag{25}$$

where K_s and μ_s are the bulk and shear moduli of the solid grains. The mesoscopic-loss effect is enhanced when the two fluids are quite different, such as gas and brine. The properties of the fluids depend on temperature and pressure, which in turn depend on depth z. The gas adiabatic bulk modulus and density can be calculated from the Peng-Robinson equation of state, while the properties of brine are given by the Batzle and Wang relations (e.g., Picotti *et al.*, 2012).

VIII. RESULTS

We consider the model of Fig. 1, where a sedimentary overburden overlies a caprock. First, we computed the petrophysical parameters of the model, and determined the P-wave velocity and quality factor versus frequency of each geological formation. Then, by fitting these curves we built the equivalent viscoelastic media and run the numerical simulations of wave propagation.

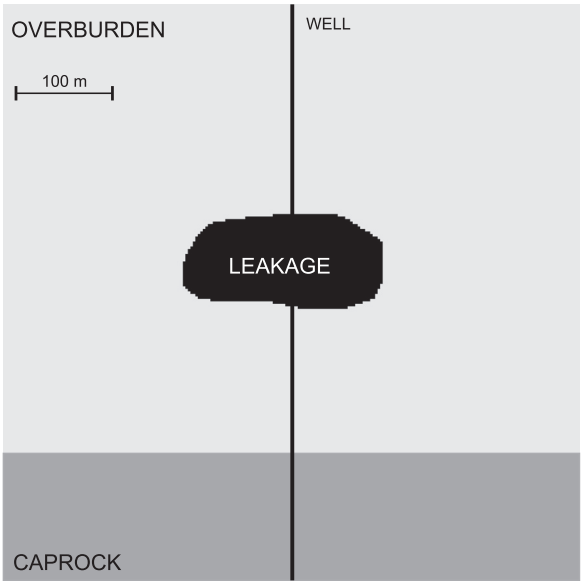

FIG. 1. Two-dimensional synthetic model of the aquifer overburden and caprock, whose material and fluid properties are given in Tables I and II.

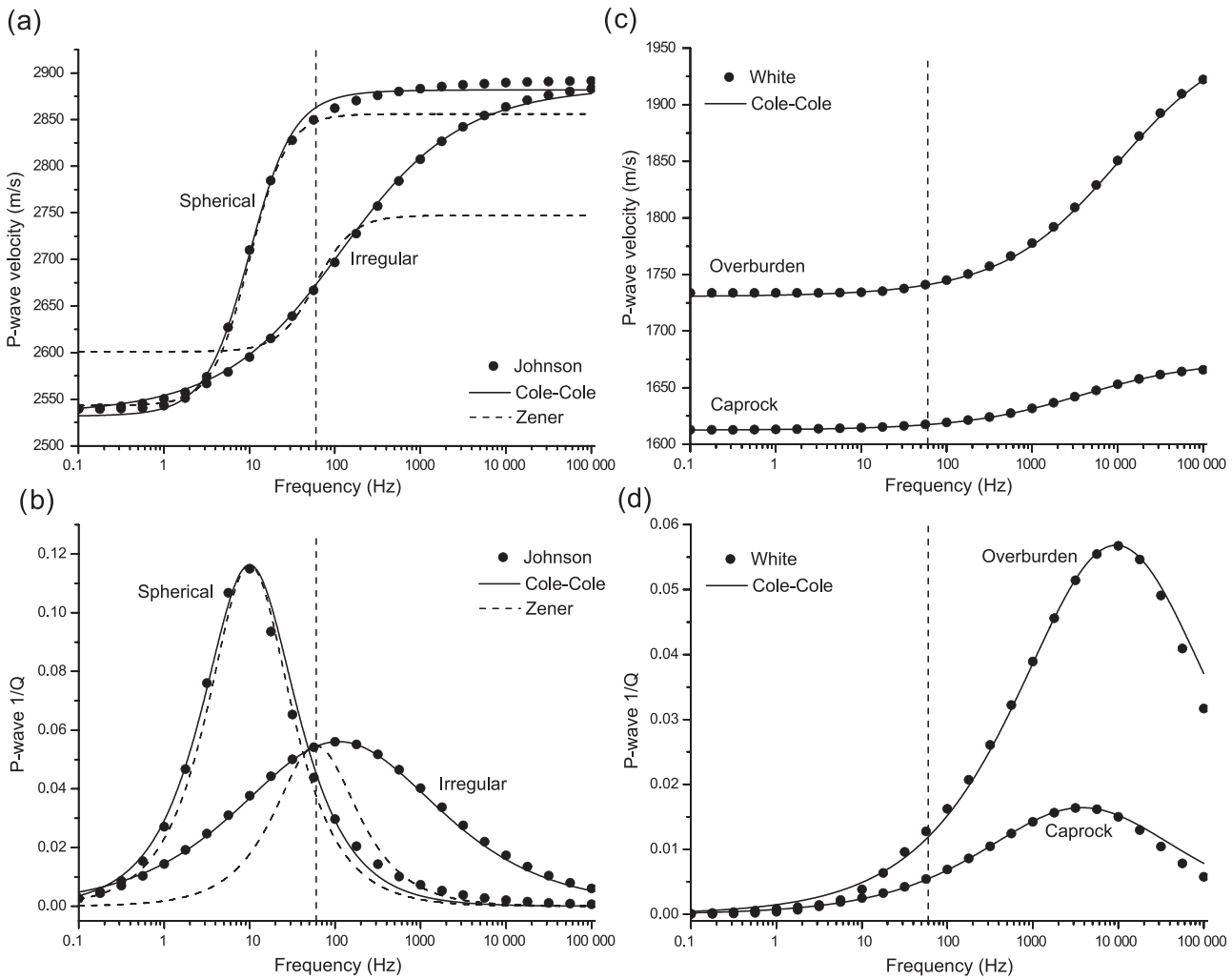

FIG. 2. Phase velocity (a) and quality factor (b) curves, corresponding to the leakage for different patch geometries, computed with the Johnson model. Phase velocity (c) and quality factor (d) curves, corresponding to the overburden and caprock, computed with the White layered model. The best fits of the Cole-Cole model were obtained using the parameters listed in Table III, while for the Zener model it is $q = 1$. The vertical dashed line indicates the dominant frequency of the source for the numerical simulation.

A. Viscoelastic model building

Both overburden and caprock consist of a periodic sequence of sandstone and mudstone thin layers with different proportions. The period of the stratification is 1 cm and 4 cm in the overburden and caprock, respectively, while the mudstone proportion is 50% in the overburden and 80% in the caprock. The porous material is fully saturated with brine, and the mesoscopic-loss effect is due to heterogeneities in the petrophysical properties of the hosting rock. Attenuation and velocity dispersion curves, shown in Figs. 2(c) and 2(d), are computed using White's layered model.

As shown in the geological model of Fig. 1, we simulate a possible CO_2 leakage caused by the degradation of the casing of an abandoned well. It is assumed that the CO_2 is accumulated in a lenticular sandstone structure in the overburden. The material and fluid properties, computed using the equations of Sec. VII, are given in Tables I and II.

Figure 2 shows the phase velocity (a) and quality factor (b) obtained by using the Johnson model and two different geometries of the patches, i.e., the concentric spheres geometry and an irregular (fractal) geometry. In the first case, a gas-saturated sphere is surrounded by an outer sphere of radius $R = 50$ cm, and the CO_2 saturation is $S_g = 10\%$. To obtain the irregular patch, we proceed as described in Picotti *et al.* (2010). We start from the spherical patch of size factor

TABLE I. Material properties.

	Sandstone	Mudstone
Grain bulk modulus, K_s (GPa)	36	12
shear modulus, μ_s (GPa)	45	6
size, D (μm)	50	1
density, ρ_s (kg/m^3)	2650	2600
Frame[a] bulk modulus, K_m (GPa)	15.6	0.16
shear modulus, μ_m (GPa)	19.5	0.08
porosity, ϕ	0.2	0.45
permeability, κ (mD)	95	0.92
Frame[b] bulk modulus, K_m (GPa)	4.93	–
shear modulus, μ_m (GPa)	6.16	–
porosity, ϕ	0.35	–
permeability, κ (D)	0.77	–

[a]Overburden and caprock.
[b]Sandstone lens.

TABLE II. Fluid properties.

	Overburden	Caprock
Brine density, ρ_w (kg/m^3)	1036	1036
viscosity, η_w (cP)	1.29	1.12
bulk modulus, K_w (GPa)	2.38	2.46
CO_2 density, ρ_g (kg/m^3)	70.9	—
viscosity, η_g (cP)	0.016	—
bulk modulus, K_g (MPa)	3.95	—

TABLE III. Viscoelastic properties.

Formation	q	ρ (kg/m^3)	c_P[a] (m/s)	Q_0	f_0 (Hz)
Overburden	0.53	2112	1968	17	9397
Leakage	0.52	2051	2885	18	110
Caprock	0.52	1982	1675	61	3772

[a]The unrelaxed P-wave velocity is $c_P = \sqrt{M_U/\rho}$.

$1000\,T = 10$ and shape factor $S/V = 1.3\,\mathrm{m}^{-1}$. Then, we deform the patch from a sphere to a fractal rough shape, by multiplying the shape factor of the initial geometry by a factor of 10. As observed by Picotti *et al.* (2010), we note that the shape of the curves corresponding to the two geometries are similar, but as the irregularity of the patches increase, the relaxation peak moves towards higher frequencies, whereas the maximum loss decreases.

With the purpose of determining the parameters of the equivalent viscoelastic media, we fit both the phase velocity and quality factor curves using the Zener and Cole-Cole models, described in Sec. III. The viscoelastic properties of the Cole-Cole model are given in Table III, where the unrelaxed P-wave velocity is $c_P = \sqrt{M_U/\rho}$. The results, displayed in Figs. 2(a) and 2(b), clearly show that while the best fit of the Zener model is satisfactory for the spherical geometry, it is inadequate for the irregular geometry. Instead, the best fit obtained using the Cole-Cole model is excellent at all frequencies. Figures 2(c) and 2(d) show that the fits are excellent also for the overburden and caprock.

B. Unbounded homogeneous medium numerical test

Analytical solutions of wave propagation problems are exact and conceptually appealing, but can be obtained only under rather restrictive assumptions about the geometry and the nature of the propagation medium. On the other hand, numerical solutions can cope with complex media and arbitrary boundary conditions, but are error prone and hence require verification (i.e., tests with synthetic data) and validation (i.e., tests with realistic data). Therefore, we first verify our numerical algorithm by comparing numerical and analytical solutions arising from a model that assumes an unbounded homogeneous model. Appendix C provides the analytical solution. To compute the numerical transient responses, we use the following time-dependence for the source:

$$s(t) = \left(a - \frac{1}{2}\right)\exp(-a), \quad a = \left[\frac{\pi(t - t_s)}{t_p}\right]^2, \tag{26}$$

where t_p is the period of the wave and we take $t_s = 1.4t_p$. Its frequency spectrum is

$$S(\omega) = \left(\frac{t_p}{\sqrt{\pi}}\right)\bar{a}\exp(-\bar{a} - \mathrm{i}\omega t_s), \quad \bar{a} = \left(\frac{\omega}{\omega_p}\right)^2,$$
$$\omega_p = \frac{2\pi}{t_p}. \tag{27}$$

The peak frequency is $f_p = 1/t_p$.

We now perform simulations to compare snapshots between a hypothetical lossless medium and the actual medium. A sandstone formation is discretized on a numerical mesh with uniform vertical and horizontal grid spacings of 3 m, and 231×231 grid points. The viscoelastic parameters are those of the leakage in Table III, but with $Q_0 = 10$. A dilatational source is applied at the center of the mesh with a peak frequency $f_p = 60$ Hz. We use a memory length $L = 70$, a time step $h = 0.2$ ms and $m = 1$. We run several simulations using $q = 0.2$, 0.5, 1, and 1.5. Figures 3(a) and 3(b) show the phase velocity and quality factor as a function of frequency, for the different values of q, respectively. It is clear that the lower is q the lossier is the medium. In particular, for $q > 1$ we obtain narrower quality factor curves respect to the Zener

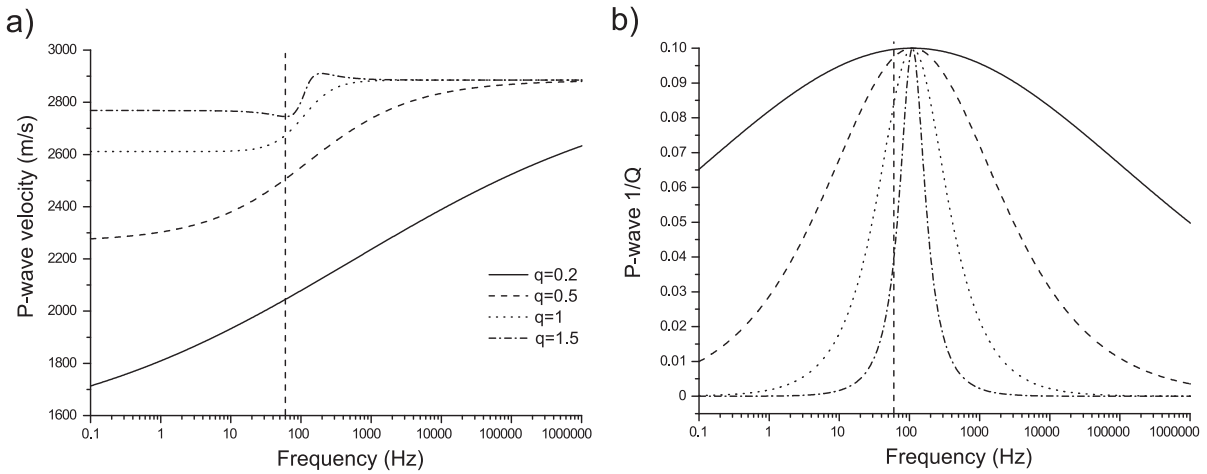

FIG. 3. Phase velocity (a) and quality factor (b) as a function of frequency, corresponding to $q = 0.2$, 0.5, 1, 1.5. The viscoelastic parameters are those of the leakage in Table III, but with $Q_0 = 10$. The vertical dashed line indicates the dominant frequency of the source for the numerical simulation.

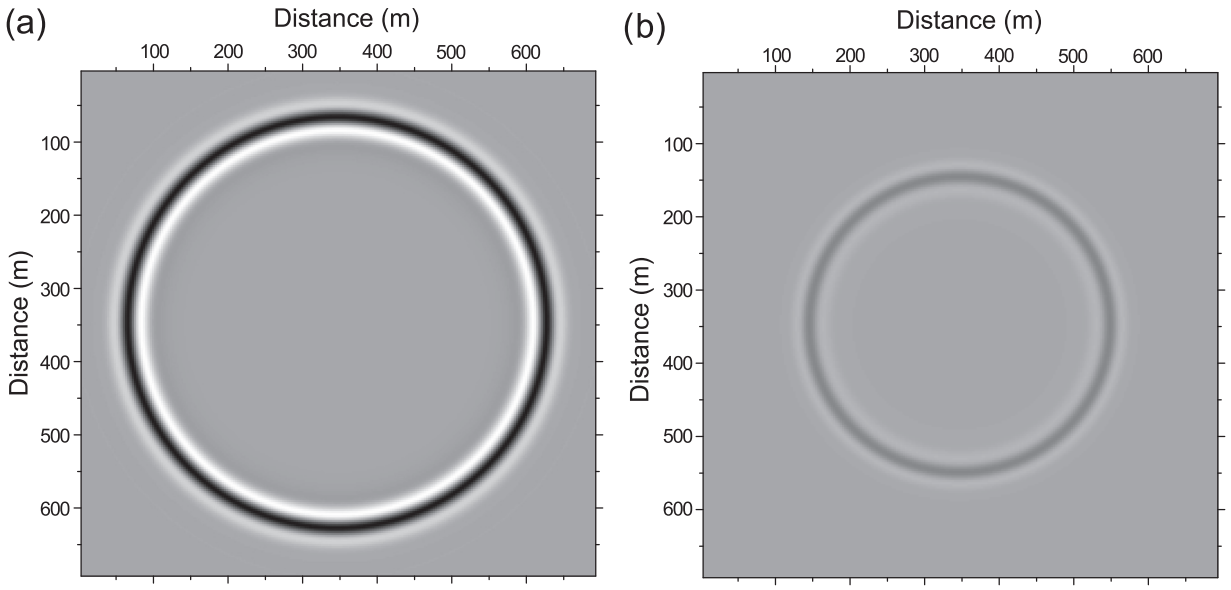

FIG. 4. Snapshots of the dilatational wave in a sandstone formation at 0.12 s, where (a) corresponds to the lossless medium ($q = 0$) and (b) to the lossy medium ($q = 0.2$ and $Q_0 = 10$). The other viscoelastic parameters are those of the leakage in Table III.

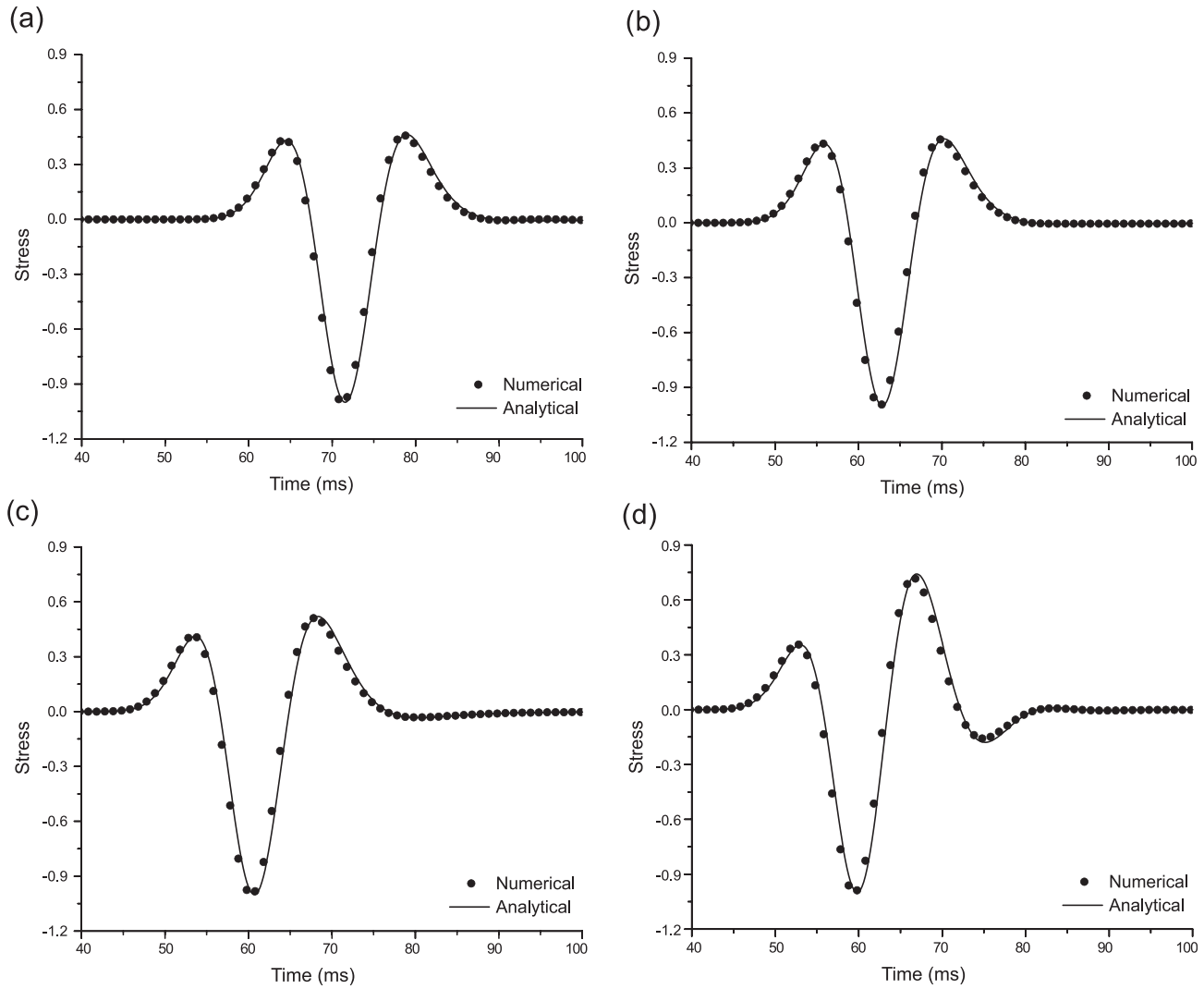

FIG. 5. Comparison between the analytical (solid line) and numerical (dots) solutions in a sandstone lossy medium, for $q = 0.2$ (a), 0.5 (b), 1 (c), and 1.5 (d). The field is normalized and the source-receiver distance is about 100 m.

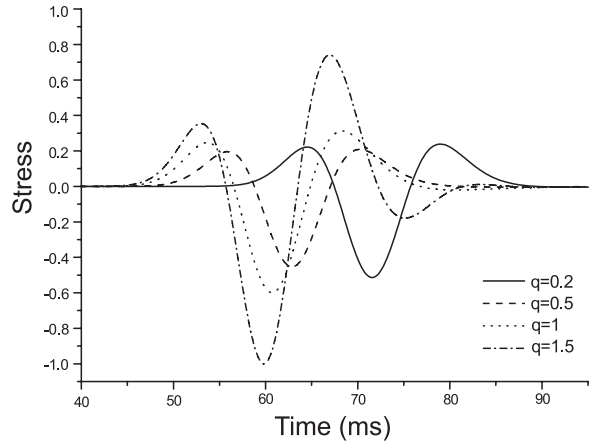

FIG. 6. Comparison between the analytical transient solutions, for $q = 0.2$, 0.5, 1, and 1.5. The source-receiver distance is about 100 m.

case ($q = 1$). On the other hand, for $0 < q < 1$ the curves are broader. In the limit of $q = 2$ the imaginary part of the Cole-Cole element vanishes and the quality factor peak reduces to a delta function centered at f_0. Figure 4 shows the snapshots at 0.12 s, where the strong attenuation and velocity dispersion in the real medium [Fig. 4(b)] is evident.

Figure 5 compares the numerical and analytical transient solutions at a distance of about 100 m from the source location. The agreement between solutions has an L^2-norm error lesser than 0.5%. Figure 6 compares the different analytical transient solutions, showing that for lower values of q the medium is more lossy and dispersive.

C. Simulation of a leakage scenario

We consider the idealized model of aquifer overburden and caprock shown in Fig. 1, with the purpose of illustrating

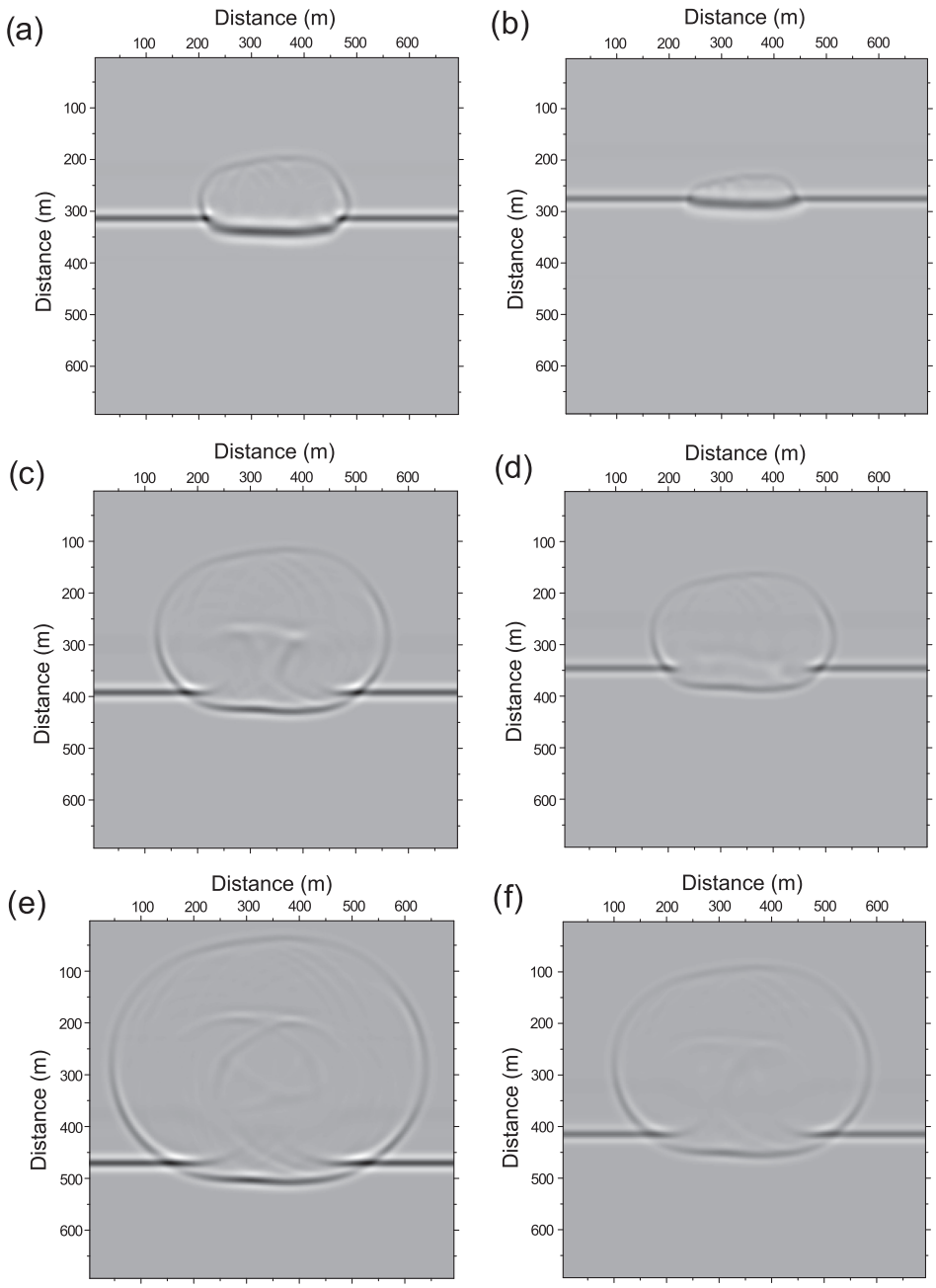

FIG. 7. Snapshots of wave field propagation in the model of Fig. 1 at 0.18 s [(a), (b)], 0.22 s [(c), (d)], and 0.26 s [(e), (f)], where panels (a), (c), (e) correspond to a hypothetical lossless medium and panels (b), (d), (f) correspond to the actual medium.

the attenuation and velocity dispersion effects due to the presence of a CO_2 leakage within the overburden. The viscoelastic parameters of each geologic formation correspond to the properties shown in Table III. The model is discretized on a numerical mesh with uniform vertical and horizontal grid spacings of 3 m, and 231×231 grid points. The mesh has absorbing boundary conditions (Cerjan *et al.*, 1985) at the top and bottom of the grid (20 grid cells). Due to the periodicity of the Fourier method, the absorbing strip of the top boundary is located at the bottom of the mesh. To be effective, the damping is applied to all the temporal levels, u^n, $n=-1$, 0, 1. To simulate the propagation of a plane wave, a dilatational source is applied at each grid cell at the top of the mesh, with a peak frequency $f_p = 60$ Hz. We use a memory length $L = 70$, a time step $h = 0.2$ ms and $m = 1$.

Figure 7 compare snapshots between a hypothetical lossless medium (a), (c), (e) and the actual medium (b), (d), (f). The snapshots show the wave field at three different propagation times, 0.18, 0.22, and 0.26 s, displaying how the down-going plane wave is diffracted by the leakage. As can be seen, the field is faster and more attenuated in the region where the leakage is present, while velocities and amplitudes in the real medium are lower than in the lossless medium. The simulations show that the seismic technique is suitable for CO_2 storage monitoring and leakage detection. This methodology allows a more reliable evaluation of the sensitivity of the seismic method to the CO_2 detection.

IX. CONCLUSIONS

We have presented a numerical algorithm to model seismic propagation in partially saturated porous media based on the Cole-Cole model, which implies the solution of fractional time derivatives of stress and strain. The kernel of this stress-strain relation has three parameters that can be obtained by fitting real or synthetic data, namely, the unrelaxed (high-frequency) velocity, the maximum dissipation factor and the fractional order. In this work, we fitted the P-wave velocity and quality factor obtained using the While and Johnson models, the latter being a generalization of White theory for patches of arbitrary shape. The wave field is computed in the time-space domain using the Grünwald-Letnikov approximation and the staggered Fourier pseudospectral method. The algorithm is successfully tested against an analytical solution and applied to CO_2 detection and monitoring. It provides an optimal description of the mesoscopic-loss effect arising in partially saturated porous media, and allows to obtain more realistic simulations of the wave propagation phenomena. In the specific example considered, this methodology enables for a better evaluation of the sensitivity of the seismic method to the CO_2 detection.

The advantages of this approach are that the viscoelastic modeling uses fewer material properties and field variables than the corresponding poroelastic modeling. Moreover, the use of very small grid spacings due to the presence of the Biot slow wave can be avoided, allowing to adopt coarser grids. This implies a considerable reduction of computer time and storage saving, particularly in three dimensions.

This research is of particular relevance for the simulation of wave propagation in reservoir rocks.

APPENDIX A: DYNAMIC BULK MODULUS AND JOHNSON'S MODEL

The dynamic bulk modulus $K(\omega)$ describes the crossover between the two frequency limits, i.e., from the Gassmann-Wood (GW) modulus at low frequencies to the Gassmann-Hill (GH) modulus at high frequencies. When the pore space is partially saturated with two very different fluids, such as gas and water, a fast P wave traveling in the medium induces very different pore pressures in the two regions, which tend to equilibrate through a diffusive phenomenon governed by the so called Biot acoustic slow-wave. The effective P-wave bulk modulus of the two regions is

$$K_E = \frac{E_m \bar{M}}{E_G} \tag{A1}$$

(Carcione and Picotti, 2006), where

$$E_m = K_m + \frac{4}{3}\mu_m \tag{A2}$$

is the dry-rock P-wave modulus, and

$$E_G = K_G + \frac{4}{3}\mu_m \tag{A3}$$

(Carcione, 2014), where K_m is the dry-rock bulk modulus and μ_m is the dry-rock shear modulus. The parameter $\bar{M}$ depends on the bulk modulus of the pore fluid K_f and is given by

$$\bar{M}(K_f) = \left(\frac{\alpha - \phi}{K_s} + \frac{\phi}{K_f}\right)^{-1}, \tag{A4}$$

where K_s is the solid-grain bulk modulus and α (also known as the Biot-Willis coefficient) is defined as

$$\alpha = 1 - \frac{K_m}{K_s}. \tag{A5}$$

The Gassmann bulk modulus K_G is given by

$$K_G = K_m + \alpha^2 \bar{M}. \tag{A6}$$

As shown by White (1975), slow-wave diffusion induces wave-velocity dispersion and attenuation of the fast P wave, which depends mostly on the size of the gas pockets (saturation), frequency, permeability and porosity of the rocks. At very low frequencies, there is enough time for pore pressure to equilibrate to a constant value. Therefore, the fluid pressure is uniform (isostress state), and the effective modulus of the pore fluid is given by Wood's modulus (Wood, 1955), K_W, which is exact for the static modulus of two fluids,

$$K_W = \left(\frac{S_1}{K_{f1}} + \frac{S_2}{K_{f2}}\right)^{-1}, \tag{A7}$$

where S_j, $j=1$, 2, is the saturation of the jth fluid. In this case, the effective bulk modulus of the composite at the low frequency limit is given by the Gassmann expression

$$K_{GW} = K_m + \alpha^2 \bar{M}(K_W) \tag{A8}$$

(e.g., Johnson, 2001), and it is independent of the spatial distribution of the fluids. The process of equilibration is governed by the diffusion equation whose diffusivity constant is given by

$$D(K_f) = \frac{\kappa K_E}{\eta}, \tag{A9}$$

and the critical fluid diffusion relaxation length is

$$L_c = \sqrt{D/\omega}. \tag{A10}$$

On the other hand, when the frequency is sufficiently high (e.g., smaller diffusion lengths) the pore pressures in the two phases do not have enough time to equilibrate within one half cycle. Consequently, the pressure is not uniform, but it can be assumed to be constant within each phase. In such a situation, the fluid flow effect can be ignored and Hill's theorem (e.g., Hill, 1964) gives the composite bulk modulus at the high-frequency limit

$$K_{GH} = \left(\frac{S_1}{E_{G1}} + \frac{S_2}{E_{G2}}\right)^{-1} - \frac{4}{3}\mu_m. \tag{A11}$$

The high-frequency P-wave modulus is given by

$$E_\infty = K_{GH} + \frac{4}{3}\mu_m. \tag{A12}$$

Johnson (2001) suggested for $K(\omega)$ the following expression:

$$K(\omega) = K_{GH} - \frac{K_{GH} - K_{GW}}{1 - \xi + \xi\sqrt{1 - i\omega\tau/\xi^2}}, \tag{A13}$$

and the P-wave modulus is

$$E(\omega) = K(\omega) + \frac{4}{3}\mu_m, \tag{A14}$$

where the parameters ξ and τ are calculated from S/V and T separately (Johnson, 2001; Picotti *et al.*, 2010). They are not fitting parameters; rather, they have a precise physical significance: ξ is a shape parameter, whereas τ sets the frequency scale. When $\xi < 1$ the crossover region is quite broad, whereas when $\xi > 1$ it is quite narrow. The parameter S/V depends on the shape of the patches, while the parameter T is governed by the mean size of the patch in a complicated and non-local way, which can be solved only with certain simplifying geometries (Johnson, 2001). Let us consider, for example, the concentric spherical geometry (White, 1975), wherein region 1 is a gas-filled sphere of porous medium of radius a surrounded by region 2 of outer water-filled sphere of radius b ($a < b$). The two Johnson parameters have the following expression:

$$S/V = 3\frac{a^2}{b^3},$$

$$T = \frac{K_{GW}\phi^2}{30\kappa b^3}\left\{\left[3\eta_2 g_2^2 + 5(\eta_1 - \eta_2)g_1 g_2 - 3\eta_1 g_1^2\right]a^5 - 15\eta_2 g_2(g_2 - g_1)a^3 b^2 + 5g_2[3\eta_2 g_2 - (2\eta_1 - \eta_2)g_1]a^2 b^3 - 3\eta_2 g_2^2 b^5\right\},$$

where

$$g_j = \frac{(1 - K_m/K_s)(1/K_W - 1/K_{fj})}{1 - K_m/K_s - \phi K_m/K_s + \phi K_m/K_W}, \quad j = 1, 2. \tag{A15}$$

APPENDIX B: WHITE'S MODEL OF A LAYERED POROUS MEDIUM

Let us consider a periodic layered system composed of porous media 1 and 2 with thickness d_l, period $d_1 + d_2$ and saturation $S_l = d_l/(d_1 + d_2)$, $l = 1$, 2. White *et al.* (1975) obtained the complex bulk modulus for a P wave traveling along the direction perpendicular to the stratification. It is given by

$$E(\omega) = \left[\frac{1}{E_\infty} + \frac{2(r_2 - r_1)^2}{i\omega(d_1 + d_2)(I_1 + I_2)}\right]^{-1}. \tag{B1}$$

Omitting the subindex l for clarity, we have for each medium,

$$r = \frac{\alpha M}{E_G}. \tag{B2}$$

This is the ratio of fast P-wave fluid tension to total normal stress. Moreover,

$$I = \frac{\eta}{\kappa k}\coth\left(\frac{kd}{2}\right) \tag{B3}$$

is an impedance related to the slow P wave, where η is the fluid viscosity and κ is the permeability, and

$$k = \sqrt{\frac{i\omega\eta}{\kappa K_E}} \tag{B4}$$

is the complex wavenumber of the slow P wave. The parameters E_∞, M, K_E and E_G are given by Eqs. (A12), (A4), (A1), and (A3), respectively.

APPENDIX C: GREEN'S FUNCTION AND ANALYTICAL SOLUTION

A 2D analytical solution corresponding to Eq. (17) with $m = 1$ in a homogeneous medium can easily be obtained. Combining the expressions, we have

$$\partial_t^2 \epsilon = \frac{1}{\rho}\Delta\sigma. \tag{C1}$$

In the frequency domain, $\sigma = M\epsilon$, according to Eq. (8), and using Eq. (17), Eq. (C1) becomes a Helmholtz equation

$$\Delta\epsilon + p^2\epsilon = -\frac{\Delta s}{\mathrm{i}\omega M\left[1 + (\mathrm{i}\omega\tau_\sigma)^q\right]}, \quad p = \frac{\omega}{\bar{v}}, \tag{C2}$$

where p is the wavenumber and $\bar{v}$ is given by Eq. (9). If v is real, the medium is lossless. The solution to the acoustic (lossless) equation $(\Delta + p^2)G = -8\delta(r)$ is the Green function $G = -2\mathrm{i}H_0^{(2)}(pr)$, with $\bar{v} = c_0$, where $H_0^{(2)}$ is the zero-order Hankel function of the second kind (e.g., Carcione, 2014). More precisely,

$$G(x, y, x_0, y_0, \omega, c_0) = -2\mathrm{i}H_0^{(2)}\left(\frac{\omega r}{c_0}\right), \tag{C3}$$

where (x_0, y_0) is the source location, and

$$r = \sqrt{(x - x_0)^2 + (y - y_0)^2}. \tag{C4}$$

The anelastic solution is obtained by invoking the correspondence principle (Bland, 1960), i.e., by substituting the acoustic velocity c_0 with the complex velocity $\bar{v}$. The differential operator $-\Delta/(\mathrm{i}\omega M[1 + (\mathrm{i}\omega\tau_\sigma)^q])$ acts on the source in Eq. (C2). Thus, the Green's function for the strain is

$$G_\epsilon = -\frac{1}{\mathrm{i}\omega M\left[1 + (\mathrm{i}\omega\tau_\sigma)^q\right]}\Delta G. \tag{C5}$$

Since $\Delta G = -p^2 G$ away from the source and $\sigma = M\epsilon$, the Green's function for the stress is

$$G_\sigma = MG_\epsilon = \frac{p^2 G}{\mathrm{i}\omega\left[1 + (\mathrm{i}\omega\tau_\sigma)^q\right]}. \tag{C6}$$

We set $G(-\omega) = G^*(\omega)$, where the superscript asterisk denotes complex conjugation. This equation ensures that the inverse Fourier transform of the Green's function is real. The frequency-domain solution is then given by $\sigma(\omega) = \frac{1}{8}G_\sigma(\omega)F(\omega)$, where F is the Fourier transform of the source time history. Hence,

$$\begin{aligned}\sigma(x, y, x_0, y_0, \omega) &= \frac{1}{8}G_\sigma F \\ &= -\frac{\omega F(\omega)}{4\bar{v}^2\left[1 + (\mathrm{i}\omega\tau_\sigma)^q\right]}H_0^{(2)}\left(\frac{\omega r}{\bar{v}}\right).\end{aligned} \tag{C7}$$

Because the Hankel function has a singularity at $\omega = 0$, we assume $G = 0$ for $\omega = 0$, an approximation that does not have a significant effect on the solution [note, moreover, that $F(0) = 0$]. The time-domain solution $\sigma(t)$ is obtained by a discrete inverse Fourier transform. We have tacitly assumed that σ and $\mathrm{d}\sigma/\mathrm{d}t$ are zero at time $t = 0$.

Abdullah, H. H., Elsadek, H. A., ElDeeb, H. E., and Bagherzadeh, N. (**2012**). "Fractional derivatives based scheme for FDTD modeling of nth-order Cole-Cole dispersive media," IEEE Ant. Wire. Propag. Lett. **11**, 281–284.

Bagley, R. L., and Torvik, P. J. (**1986**). "On the fractional calculus model of viscoelastic behavior," J. Rheol. **30**, 133–155.

Bano, M. (**2004**). "Modelling of GPR waves for lossy media obeying a complex power law of frequency for dielectric permittivity," Geophys. Prospect. **52**, 11–26.

Batzle, M., De-Hua, H., and Hofmann, R. (**2006**). "Fluid mobility and frequency-dependent seismic velocity—Direct measurements," Geophysics **71**, N1–N9.

Bia, P., Caratelli, D., Mescia, L., Cicchetti, R., Maione, G., and Prudenzano, F. (**2015**). "A novel FDTD formulation based on fractional derivatives for dispersive Havriliak-Negami media," Sign. Process. **105**, 312–318.

Bland, D. R. (**1960**). *The Theory of Linear Viscoelasticity* (Pergamon, Oxford).

Caputo, M., Carcione, J. M., and Cavallini, F. (**2011**). "Wave simulation in biological media based on the Kelvin-Voigt fractional-derivative stress-strain relation," Ultrasound Med. Biol. **37**, 996–1004.

Carcione, J. M. (**1998**). "Viscoelastic effective rheologies for modeling wave propagation in porous media," Geophys. Prospect. **46**, 201–352.

Carcione, J. M. (**1999**). "Staggered mesh for the anisotropic and viscoelastic wave equation," Geophysics **64**, 1863–1866.

Carcione, J. M. (**2009**). "Theory and modeling of constant-Q P- and S-waves using fractional time derivatives," Geophysics **74**, T1–T11.

Carcione, J. M. (**2014**). *Wave Fields in Real Media. Theory and Numerical Simulation of Wave Propagation in Anisotropic, Anelastic, Porous and Electromagnetic Media*, 3rd ed., revised and extended (Elsevier Science, Amsterdam).

Carcione, J. M., Cavallini, F., Mainardi, F., and Hanyga, A. (**2002**). "Time-domain seismic modeling of constant Q-wave propagation using fractional derivative," Pure Appl. Geophys. **159**, 1719–1736.

Carcione, J. M., and Gurevich, B. (**2011**). "Differential form and numerical implementation of Biot's poroelasticity equations with squirt dissipation," Geophysics **76**, N55–N64.

Carcione, J. M., and Picotti, S. (**2006**). "P wave seismic attenuation by slow-wave diffusion: Effects of inhomogeneous rock properties," Geophysics **71**, 1–8.

Cerjan, C., Kosloff, D., Kosloff, R., and Reshef, M. (**1985**). "A non reflecting boundary condition for discrete acoustic and elastic wave equations," Geophysics **50**, 705–708.

Cole, K. S., and Cole, R. H. (**1941**). "Dispersion and absorption in dielectrics. I. Alternating current characteristics," J. Chem. Phys. **9**, 341–351.

Grimnesand, S., and Martinsen, Ø. G. (**2005**). "Cole electrical impedance model—A critique and an alternative," IEEE Trans. Biomed. Eng. **52**, 133–135.

Hanyga, A. (**2003**). "An anisotropic Cole-Cole model of seismic attenuation," J. Comput. Acoust. **11**, 75–90.

Hill, R. (**1964**). "Theory of mechanical properties of fiber-strengthened materials," J. Mech. Phys. Solids **11**, 357–372.

Krief, M., Garat, J., Stellingwerff, J., and Ventre, J. (**1990**). "A petrophysical interpretation using the velocities of P and S waves (full waveform sonic)," Log Anal. **31**, 355–369.

Johnson, D. L. (**2001**). "Theory of frequency dependent acoustics in patchy-saturated porous media," J. Acoust. Soc. Am. **110**, 682–694.

Lu, J.-F., and Hanyga, A. (**2004**). "Numerical modelling method for wave propagation in a linear viscoelastic medium with singular memory," Geophys. J. Int. **159**, 688–702.

Mavko, G., Mukerji, T., and Dvorkin, J. (**1998**). *The Rock Physics Handbook: Tools for Seismic Analysis in Porous Media* (Cambridge University Press, New York).

Müller, T. M., and Gurevich, B. (**2005**). "Wave-induced fluid flow in random porous media: Attenuation and dispersion of elastic waves," J. Acoust. Soc. Am. **117**, 2732–2741.

Picotti, S., Carcione, J. M., Gei, D., Rossi, G., and Santos, J. E. (**2012**). "Seismic modeling to monitor CO_2 geological storage: The Atzbach-Schwanenstadt gas field," J. Geophys. Res. **117**, B06103, doi:10.1029/2011JB008540.

Picotti, S., Carcione, J. M., Rubino, G., and Santos, J. E. (**2007**). "P-Wave seismic attenuation by slow-wave diffusion: Numerical experiments in partially saturated rocks," Geophysics **72**, N11–N21.

Picotti, S., Carcione, J. M., Rubino, G., Santos, J. E., and Cavallini, F. (**2010**). "A viscoelastic representation of wave attenuation in porous media," Comput. Geosci. **36**, 44–53.

Podlubny, I. (**1999**). *Fractional Differential Equations* (Academic, San Diego).
Rekanos, I. T., and Yioultsis, T. V. (**2014**). "Approximation of Grünwald-Letnikov fractional derivative for FDTD modeling of Cole-Cole media," IEEE Trans. Magn. **50**, 181–184.
Revil, A., and Florsch, N. (**2010**). "Determination of permeability from spectral induced polarization data in granular media," Geophys. J. Int. **181**, 1480–1498.
Revil, A., Florsch, N., and Camerlynck, C. (**2014**). "Spectral induced polarization porosimetry," Geophys. J. Int. **198**, 1016–1033.
Revil, A., and Jardani, A. (**2010**). "Seismoelectric response of heavy oil reservoirs: theory and numerical modelling," Geophys. J. Int. **180**, 781–797.
Revil, A., Leroy, P., Ghorbani, A., Florsch, N., and Niemeijer, A. R. (**2006**). "Compaction of quartz sands by pressure solution using a Cole-Cole distribution of relaxation times," Geophys. J. Int. **111**, B09205.
Spencer, J. W. (**1981**). "Stress relaxations at low frequencies in fluid-saturated rocks: Attenuation and modulus dispersion," J. Geophys. Res. **86**, 1803–1812, doi:10.1029/JB086iB03p01803.
White, J. E. (**1975**). "Computed seismic speeds and attenuation in rocks with partial gas saturation," Geophysics **40**, 224–232.
White, J. E., Mikhaylova, N. G., and Lyakhovitskiy, F. M. (**1975**). "Low-frequency seismic waves in fluid saturated layered rocks," Izv. Acad. Sci. USSR, Phys. Solid Earth **11**, 654–659.
Wood, A. W. (**1955**). *A Textbook of Sound* (MacMillan, New York).